EROSION OF MATERIALS USED ON SATELLITE EXTERNAL SKIN BY ELECTRIC PROPULSION

T. Tondu[1], V. Viel-Inguimbert[1], F. Darnon[2]
[1] ONERA/DESP 2, Avenue Edouard Belin, 31 055 Toulouse Cédex, France
[2] CNES 18, Avenue Edouard Belin 31 401 Toulouse Cédex, France

1   INTRODUCTION

The plume of Stationary plasma thrusters (SPT) is a divergent plasma of energetic Xe^+ ions [1], [2]. These ions are susceptible to impinge parts of satellites, in particular solar arrays. Xe ions cause erosion of exposed materials and risk to change their properties. Spacecraft surface erosion can also produce contamination, which can dramatically alter properties of surfaces such as optical transmission of cover glasses or thermal properties of thermal control coatings. Prior to this contamination study, it is very important to characterise the behaviour of materials used on satellites submitted to high energy ion bombardment. Most of the studies concerning erosion of materials are based on measurements performed in the plume of a thruster [3], [4].These studies require a quite heavy experimental set up. In order to obtain results in more flexible conditions an experimental set-up was built at the ONERA/DESP allowing to reproduce the erosion phenomena. We collected data on different materials to help the prediction of the evolution of materials in real conditions. In this paper, after a detailed presentation of the experimental set up and a description of the protocols, we expose some results obtained with Kapton® at 300eV. We study the incidence dependence on the erosion rate and on the evolution of the optical properties. Finally, we try to explain the reasons for the optical property changes.

2   DESCRIPTION OF THE EXPERIMENTAL SET-UP

2.1   Experimental set-up for erosion measurements

The experimental set-up is made of a cylindrical chamber equipped with an ion source allowing to create a flux of accelerated ions from 50 to 1200 eV. This ion flow is neutralised at the source exit by an electron-emitting filament. We obtain in the chamber a plasma flow whose velocity corresponds to the ion energy, this flow presents a certain divergence which depends on the ion energy. The total ion current given by the source is a few tens of mA. The figure 1 presents a schematic top view of the experimental set-up.
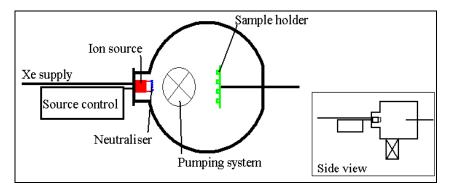

figure 1 : schematic view of the experimental set-up

The dimensions of the chamber are 50 cm of diameter and 50 cm of height. The pumping system is constituted with a primary mechanical pump and a diffusion oil pump equipped with a liquid nitrogen trap, allowing the vacuum to reach 10^{-6} hPa. When the source is operating, the pressure reaches 10^{-4} hPa.
The gas ionised is Xenon and it is introduced through a mass flow controller and the usual flow is 0,6 sccm.
The samples holder used can hold 8 samples exposed to 8 different angles at the same time. These angles are 5°, 20°, 40°, 46°, 52°, 58°, 64° and 75°.

2.2 Modification of the experimental device for contamination measurements

This vacuum chamber can be adapted to contamination experiments. The sample holder is then replaced by a large target of material bombarded by the ion flux and samples are positioned out of the beam but in front of the target. An example of such experiment can be seen on figure 2. The samples are placed on 3 sample holders maintained at a controlled temperature by a fluid circulation.
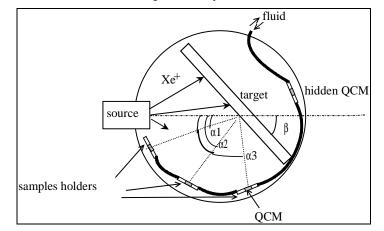

figure 2 : Schematic top view of the chamber during contamination test.

The angles of incidence $\alpha_1 = 30°$, $\alpha_2 = 90°$ and $\alpha_3 = 150°$ can be slightly modified. Each sample holder can hold 6 different samples of dimensions 15mm X 20mm and in the middle of the sample holder, a quartz micro-balance is used to monitor in real-time the deposited mass.

This experimental set-up has been validated but the results are not reported in this paper.
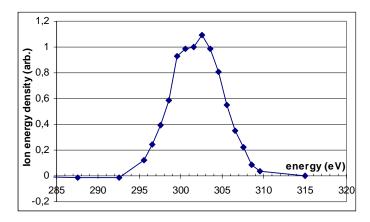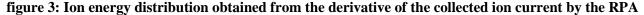
3 CHARACTERISATION OF THE ION BEAM

The characterisation of the plasma generated by the source was performed with different methods : An energy analysis was performed with a Retarding Potential Analyser (RPA) and the spatial distribution of the ion density was performed by Langmuir probe measurements.

3.1 Energy analysis

A three-grid electrostatic analyser was designed and constructed at the DESP to measure the energy distribution of drifting ions on the source centre line. In these RPA measurements the ion drifting current is collected while all plasma electrons and secondary electrons are repelled by two intermediate grids.

The ion energy distribution shown in figure 3 is approximately a Gaussian with average 301.5eV and a width at half height of 8.0 eV. The source was operated at theoritical 300 V acceleration. Therefore, the ion beam is not perfectly monoenergetic but exhibit a small energy distribution.

figure 3: Ion energy distribution obtained from the derivative of the collected ion current by the RPA

3.2 Current measurement

The evaluation of the ionic current is made with plane Langmuir probe. Since samples in the chamber take the floating potential V_f, we search the energetic ion current at this potential. The current collected by the probes has three components (figure 4).

- The energetic ions that are only slightly deviated by the probe are the first one. This current does not depend on the potential of the probe. This is the current that we want to evaluate because it corresponds to the ions responsible of erosion.

- Low energy ions (produced by charge exchange collisions between fast ions and residual Xenon atoms producing fast neutral and slow ions) are collected by the probe for negative potentials. The energetic ionic current is thus over estimated. But [6] has shown that this overestimation is compensated by fast neutrals that participate in the erosion.

- Finally, electrons are mainly collected for positive polarisation.

So we calculate the asymptote of the ionic branch of the characteristic (negative potential) and we consider that the value taken by this asymptote at the floating potential (I=0) is the current of energetic ions corresponding to the flux received by the sample.
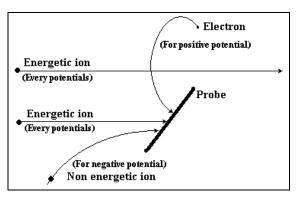

figure 4: Origins of the currents collected by the probe.

The graph presented on figure 5 shows an example of the calculation of the current received by a probe. In this example, the ionic current collected by the probe is 145µA.
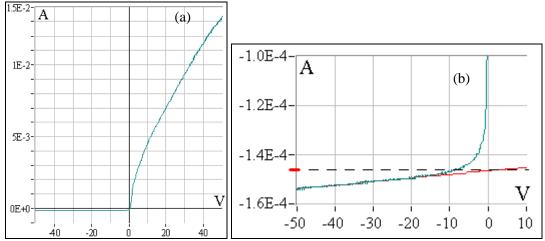

figure 5 : example of the characteristic (a) and detail of this characteristic (b)

3.3 Current Spatial dispersion

As we expose several samples (at different positions) to the ion beam in a same experiment, it is interesting to study the current density out of the source axis. This measurement was performed with

different probes placed on a horizontal axis in front of the source. The result shows a gaussian-like dispersion of the current density. (see figure 6)
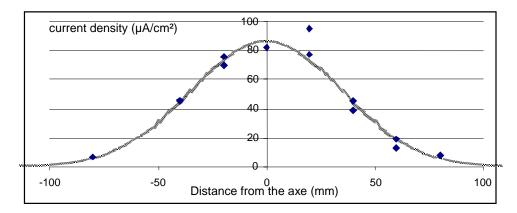

figure 6 : Ion current densities (10mA, energy : 300eV, measured at 265mm from the ion source). Experimental data seem to follow a gaussian distribution

Some parameters of the source allow to change the dispersion of the beam. Generally, we try to have the thinnest dispersion as possible. But for low energies, the dispersion is larger.

4   EXPERIMENTS

Different measurements can be made on eroded samples. The main ones are the determination of the erosion rate and the study of the optical properties of eroded samples. These two parameters can help to predict the evolution of materials in real conditions.

4.1   Erosion rate

The sputtering yield is a classical characterisation of the erosion rate [5]. Its definition is

$$\gamma = \frac{Sputtered\ Atoms}{Incident\ Ions}$$

The sputtering yield is very convenient for simple materials like metals, but less for compounds like alloys or oxides. The notion of sputtered atom does not describe the phenomenon with polymers, so that we decided to characterise the erosion rate in mm^3/C.

The measurement of erosion is performed by mass loss measurement and current evaluation. The current corresponds to the ionic flux described in §3.2. We calculate the erosion rate by:

$$\gamma_V = \frac{-\Delta m \cdot 1000}{\rho \cdot J \cdot t \cdot S} \quad mm^3 C^{-1}$$

Where Δm is the mass loss in g, ρ is the specific mass in $g.cm^{-3}$, J is the ion current density in $A.cm^{-2}$, t the duration of the experiment in s and S the surface of the sample in cm^2.

For low erosion materials, a high precision is necessary for the weight measurement. The balance used has an accuracy of $\pm20\mu g$. Some materials outgas at low pressure, and some adsorb humidity from the air. These two phenomena make the measurement sensitive to the weighing protocol. As a consequence, we perform an outgasing of the samples before the weighing : before and after the erosion. The outgasing is performed in a vaccum oven during 24 hours at 80°C under a pressure lower than 1 mbar.

For conducting samples, the measurement of the current can be performed during the erosion. The sample is used as Langmuir probe. But this is impossible with insulators. In this case, before each erosion experiment, we perform a calibration using Langmuir probes instead of the samples. Then we consider that the current is the same during the calibration and the erosion.

We use five extra probes during the experiments (centre, top, bottom, left side and right side of the beam) to control that the beam keeps the characteristics, it had during the calibration.

4.2 Optical measurement

The optical characterisation of a sample is performed using a spectrophotometer Perkin Elmer Lambda 900 equipped with an integrating sphere. This instrument allows the experimenter to measure both total (diffuse and specular) transmission and reflection of samples in the solar spectrum range (250-2500nm).

The solar absorptance α_s is the integration of the absorptance over the solar spectrum and is calculated following the equation :

$$\alpha_s = \frac{\int_{\lambda_1}^{\lambda_2} \alpha(\lambda)\ S(\lambda)\ d\lambda}{\int_{\lambda_1}^{\lambda_2} S(\lambda)\ d\lambda}$$

where: $\alpha(\lambda)=1-[R(\lambda)+ T(\lambda)]$
$R(\lambda)$ = spectral reflectance after 100% reference correction
$T(\lambda)$ = spectral transmittance
$S(\lambda)$= spectral solar irradiance.(ref : ASTM E 490-73 a).
λ_1= 0.25 µm, λ_2= 2.5 µm and dλ= 2 nm
(The solar spectrum taken between 250 and 2500 nm covers 96% of the total energy).

5   VALIDATION OF THE EROSION PROTOCOL

Literature exhibit many measurements performed on metals. Most of them have an important sputtering yield. As a consequence, they are good candidates for the verification of our protocol. According to [4] the sputtering yield for silver by Xe ions with an energy of 300eV and an incidence of 0° (see graph (b) of figure 7) is approximately 2 atom/ion. We performed an erosion experiment on silver for different erosion angles. The results are summarized in the graph (a) of the figure 7. Our measurement fits rather well with the literature.
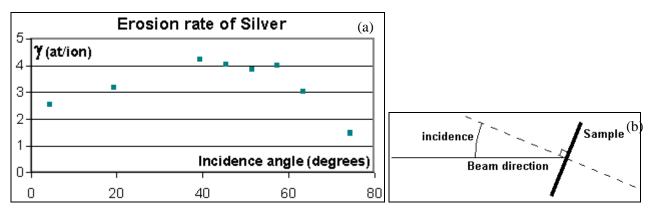

figure 7 : Measured erosion rates for different incidences

6   RESULTS ON KAPTON®

Kapton® is a polyimide produced by Dupont, widely used on satellites but rarely quoted in the literature (as for most of polymer) for what concerns erosion. So we have studied the erosion rate of kapton® under Xenon ion bombardment and measured its dependence with the ion incidence angle. We have also studied the evolution of the optical properties as a function of ion incidence angles.

6.1   Erosion rate

The erosion rate measurement was performed using 8 samples of Kapton® with the angle of incidence of 5°, 20°, 40°, 46°, 52°, 58°, 64° and 75°. As the erosion rate of Kapton® is very low, the precision is limited by the low mass loss. This measurement is also made difficult by the desorption of solvents by

Kapton® and the adsorption of water after outgassing. The results are summarised in the graph (a) of the figure 8.

The samples received a fluence between 0.4 and 2.5 C/cm^2 (depending on the angle of incidence and the position in the chamber). The calculated erosion at 5° is negative. This has no physical signification but shows how difficult the measurement is made because of solvent desorption and water adsorption. In case of low erosion, a longer exposure of the samples should lead to a better accuracy.

Calculations from the data collected by [4] induce an erosion rate of 1.4 10^{-3} mm^3/C for an incidence of 0°. This value is very low and explains our problems of measurement for low incidence. This value was obtained with a fluence of 241 C/cm^2 and this high fluence can help to increase the precision of the result.

The comparison of the silver erosion yields (figure 8) and Kapton® shows that the Kapton® has a very low erosion rate. This can be explained by the fact that Kapton® is composed of small atoms that interact less with Xe than Ag atoms. The bonds between the atoms of Kapton® are covalent and this type of bond is stronger than metallic bonds. In most of the case, the braking of one bond does not allow to break the polymer chain (see figure 9). And finally, Kapton® chains interact one with the other. This prevents the elimination of end of chains that could be cut by Xe ions.
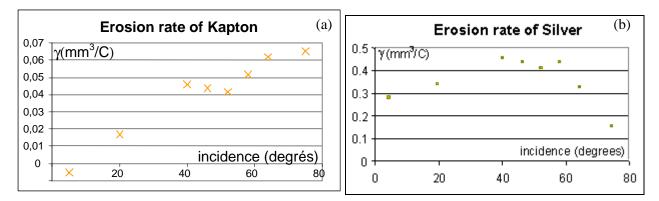

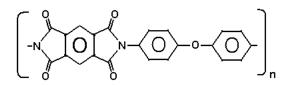figure 8 : Erosion rates of Kapton® (a) and silver (b)

figure 9 : Structure of the Kapton® chain.

6.2 Effect of the erosion on optical properties

6.2.1 Optical properties of non eroded Kapton

The erosion has an effect on the optical properties of the Kapton®. The measurements were performed on 75µm Kapton®. The graphs of figure 10 shows the transmittance (a), the reflectance (b) and the sum of transmittance and reflectance (c). We can see that Kapton® absorbs light under 500nm, but it is a perfectly transparent material between 800 and 1600nm.

Dupont gives a value of 1.66 for the refractive index of kapton. According to Frenel's laws the value for a single reflection is 6.15%. This allows with a flat film to collect up to 11,6% with multiple reflections. We expected a plateau at approximately 11,6% over 800 nm except of IR harmonic bands (this is almost verified) and another one at approximately 6.15% under 500nm. So the main difference between an ideal prediction and the real spectrum is an increase of the reflectance under 500nm down to 250nm. This is certainly caused by a diffusion phenomenon. We will see later that measurements out of the specular reflection direction shows that there is no diffusion inside the film (figure 16).
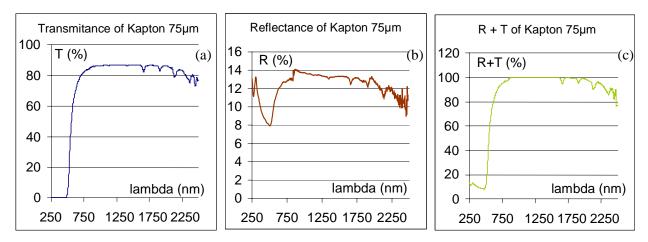
figure 10 : Transmittance (a), reflectance (b) and sum of the two (c) for Kapton 75µm

6.2.2 *Reflectance of eroded samples*

We eroded kapton samples and measured the transmittance and the reflectance. The effect of erosion on the optical properties of Kapton® is only evident for the reflection spectra, mostly in the UV-Vis region. The effect on the sum R+T is noticed in the UV-Vis part and is mainly controlled by the evolutions of the reflection. As a consequence, we will focus on the reflectance spectra.

With a normal incidence, we performed the erosion with different fluences to know how fast the evolution of reflectance occurs. With a normal incidence, we don't measure a sensitive difference between a fluence of 0.065C/cm^2 and 1.35C/cm^2. These results are displayed on the graph of the figure 11. The further results will however be obtained for fluences above 1.35C/cm^2 in order to increase the accuracy of mass loss measurements.

The figure 12 (a) shows the reflectance after an erosion under different incidences. With grazing incidence the reflectance is reduced. For normal incidence, the reflectance increases. The variation of reflectance compared with a standard that is a non eroded sample is displayed in the figure 12 (b). With grazing incidence, the reflectance tends to reach a plateau for wavelength under 500nm. The spectrum approaches the predicted spectrum for an ideal film. For normal incidence, the evolution is in the other way.
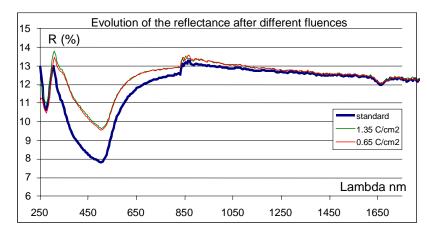

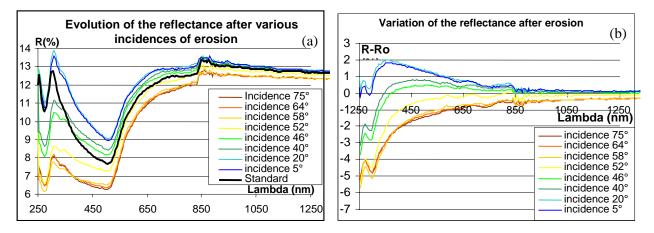**figure 11 : Evolution of the reflectance after different fluences of normal erosion.**

7

figure 12 : (a) reflectance spectra obtained on eroded samples; (b) differential spectra (R – R_standard)

6.2.3   Solar absortance

Solar absorptance of the samples was calculated from previous measurements following the equation given in paragraph 4.2. For non eroded Kapton, the value found was α_s =0.31. The evolution of the optical properties leads to a modification of the solar absorptance of eroded samples since for each angle of incidence, the solar absorptance increases. The graph of the figure 13 shows how the solar absorption evolves for different incidences.
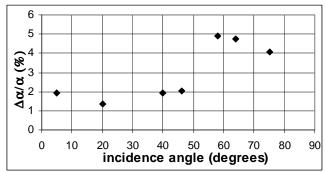

figure 13: Evolution of solar absortance of eroded samples.

For low incidence, a transmittance loss dominates the phenomenon, while for high incidences, the loss of reflectance dominates it.

6.3   Additional analysis

In this paragraph, several analysis performed in order to find an explanation to the variation of reflectance are reported. Phenomena of absorption, diffusion or surface layer could explain the variations. For one incidence, the evolution of the reflectance is not monotonous with varying wavelengths. This could indicate that two or more parameters are modified by the erosion.

When the kapton is transparent, the erosion has an effect on the reflectance measured on the non eroded face. This is due to the multiple reflections. The variations of measured reflectance is represented for the extreme incidences on figure 14. For the back face, the effect is a loss of reflectance for every incidences.

We calculated an "intrinsic transmittance". It represents the part of non reflected light that pass through the sample. The "intrinsic transmittance" or T_i is calculated by

$$T_i = \frac{T}{1-R}$$

So T_i is linked to the absorbency through the film. The evolution of T_i is displayed in the graph of the figure 15. For every incidences, the absorption of the film is slightly increased but this effect is more significative for low incidences. The variation of the reflectance of the back face and of the intrinsic

8

transmittance are opposite. This allows to say that evolutions of reflectance are not only caused by absorption phenomena. So we attribute this reflectance loss for the back face to surface diffusion of the second reflection on the eroded surface (grazing incidence). This diffusion could induce loss of light on sample's edges.

On the other hand, it should be noted that the transmittance loss is larger for a normal incidence than for a grazing incidence. This can be explained by the formation of a partially absorbent layer at the top of the material. In the case of normal incidence, the depth of penetration of Xe ions is higher than for grazing incidences. It means that the layer affected by Xe is thicker.
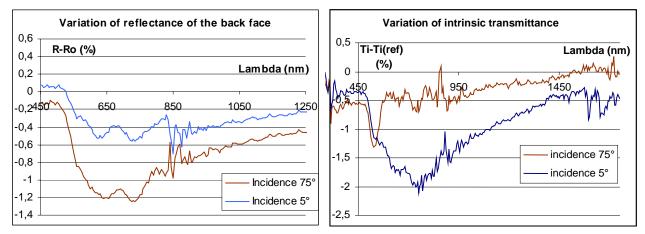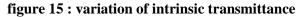

figure 14 : **Variation of the Reflectance of the back face**

figure 15 : **variation of intrinsic transmittance**

In order to confirm the influence of a diffusive part in the reflectance, we studied the proportions of diffuse and specular reflections. For this, we measured the reflectance of the samples in the same integrating sphere as before but using a light trap to remove the specular part of the reflection. This trap is quite large, so that we loose some diffuse light that is emitted close from the specular direction. The spectra ($R_{total} - R_{specular}$) of the standard (non eroded) and the extreme incidences (5° and 75°) are displayed on figure 16. From the standard, we can conclude that the Kapton is a mainly specular material in this range of wavelengths. The slight diffusion can be explained by the presence of bubbles in the film.
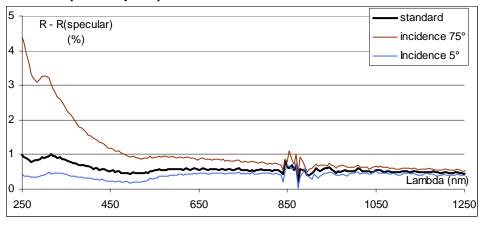

figure 16 : **Light intensity measure out of the specular direction.**

On the opposite, we observe a diffusion phenomenon in the UV range for the grazing eroded sample. This has been confirmed by surface morphology analysis : AFM analysis of the surface shows that the surface morphology is strongly dependent on the incidence of erosion. Main results are displayed in figure 17 . The 3D map represent 1µm². The profile gives the height of the roughness. Beware of the scale that are different.

We can see that the roughness of non eroded Kapton is irregular. The measured RMS roughness value is Rq=2.0 nm.

9

The formation of surface structures by ion erosion is well known [7] For an almost normal incidence (20°), we observe a homogenous roughness. The RMS roughness (Rq=1.2nm) is smaller than for non eroded Kapton . For grazing incidence (75°), the RMS roughness is more pronounced (Rq=10.5) and form non symmetrical hills. The scale of this roughness is much larger in this later case.
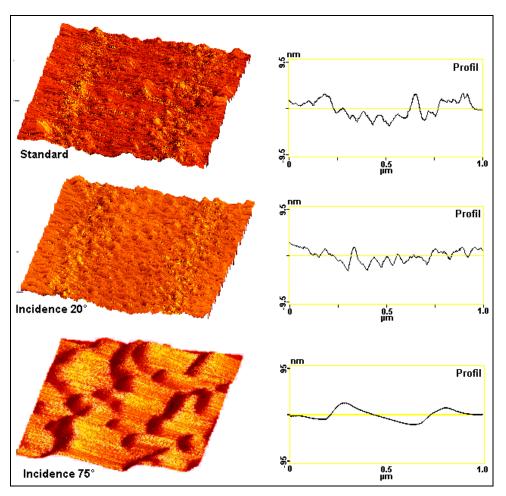

figure 17 : AFM measurements of standard and eroded (20° and 75°) surfaces

The surface characterisation has evidenced correlation between the surface topology and optical properties of the material. This explains the diffusion measurements, but it is hardly to find a clear explanation on the correlation between surface topology and total reflectance.

7   CONCLUSION

In this paper we describe a set up that allows to perform ion erosion experiments. The aim of these experiments is to foresee and understand the behaviour of materials in the plume of a plasma thruster. We illustrate this study by the case of Kapton® which is used on solar generator and which is subjected to receive energetic Xe^+ ions. The experimental set-up allows to measure precisely the erosion rate as a function of ion incidence angle. This kind of data is useful to be implemented in plume effect models in order to foresee the thickness of material that will be eroded on spacecraft surfaces, for example for the sizing of thin layers. Before and after erosion, the materials are characterised in order to determine their surface property evolutions due to erosion. For instance, it has been shown that the solar absorptance is modified when the material is eroded. This is an important point to consider in thermal control calculations. The evolutions of the optical properties of eroded materials are not completely explained, but it has been evidenced that the surface morphology plays an important role in the reflection phenomena.

This work on kapton erosion has been extended to other thermal control coatings, solar array materials and other materials used on board spacecrafts as well as to the characterisation of contamination. Now the

work is focussed on the fine investigation of the physical processes involved during erosion and contamination in order to better understand the consequences on the surface physical property changes.

8 ACKNOWLEDGEMENTS

9 REFERENCES

[1] L. B. King, A. D. Gallimore *"Ionic and Neutral Particle Transport Property Measurements in the Plume of an SPT-100"* AIAA-96-2712, Joint Propulsion Conference, July 1-3, 1996 / Lake Buena Vista, Fl.

[2] F. Darnon " *The SPT-100 Plasma Plume and its interaction with a spacecraft, from Modeling to Ground and Flight Characterization"* AIAA-00-3525, Joint Propulsion Conference, July 17-19, 2000 / Huntsville, AL.

[3] E. J. Pencil, T. Randolph, D. Manzella*, "End-of-life Stationry Plasma Thruster Far-Field Plume Characterisation"* AIAA 96-2709, Joint Propulsion Conference, July 1-3, 1996 / Lake Buena Vista, Fl.

[4] J.M. Fife, W.A. Hargus Jr, D.A. Jaworske, C. Sarmiento, L. Mason, R. Jankovsky, J.S. Snyder, S. Malone, J. Haas, G. Gallimore " *Spacecraft Interaction Test Results of High Performance Hall System SPT-140"* AIAA-2000-3521 , Joint Propulsion Conference, July 19-19, 2000 / Huntsville, Al.

 [5] R. Behrisch *Sputtering By Particle Bombardment* I, Springre-Verlag Berlin Heidelberg New York 1981

[6] Y. Garnier : thesis of the ENSAE " *Pulvérisation ionique de matériaux céramiques dans le cadre de la caractérisation d'un propulseur à effet hall*".

[7] R. Behrisch *Sputtering By Particle Bombardment* II, Springre-Verlag Berlin Heidelberg New York 1983